SecureV2X: An Efficient and Privacy-Preserving System for Vehicle-to-Everything (V2X) Applications

Joshua Lee
jlee246@ucsb.edu
University of California Santa Barbara
Santa Barbara, CA, USA

Ali Arastehfard
ali.arastehfard@uconn.edu
University of Connecticut
Storrs, CT, USA

Weiran Liu
weiran.lwr@alibaba-inc.com
Alibaba Group
China

Xuegang Ban
banx@uw.edu
University of Washington
Seattle, WA, USA

Yuan Hong
yuan.hong@uconn.edu
University of Connecticut
Storrs, CT, USA

Abstract

Autonomous driving and V2X technologies have developed rapidly in the past decade, leading to improved safety and efficiency in modern transportation. These systems interact with extensive networks of vehicles, roadside infrastructure, and cloud resources to support their machine learning capabilities. However, the widespread use of machine learning in V2X systems raises issues over the privacy of the data involved. This is particularly concerning for smart-transit and driver safety applications which can implicitly reveal user locations or explicitly disclose medical data such as EEG signals. To resolve these issues, we propose SecureV2X, a scalable, multi-agent system for secure neural network inferences deployed between the server and each vehicle. Under this setting, we study two multi-agent V2X applications: secure drowsiness detection, and secure red-light violation detection. Our system achieves strong performance relative to baselines, and scales efficiently to support a large number of secure computation interactions simultaneously. For instance, SecureV2X is 9.4× faster, requires 143× fewer computational rounds, and involves 16.6× less communication on drowsiness detection compared to other secure systems. Moreover, it achieves a runtime nearly 100× faster than state-of-the-art benchmarks in object detection tasks for red light violation detection.[1]

Keywords

Privacy, Drowsiness Detection, Red-light Violation Detection, Vehicle-to-Everything (V2X)

1 Introduction

Vehicle-to-everything (V2X) technology has played a pivotal role in enhancing road safety, optimizing traffic flow, and enabling autonomous driving technologies. Recently, the US Department of Transportation (USDOT) released its National Deployment Plan of V2X technologies [21], calling federal/state/local transportation agencies, the private sector, and researchers to work together to research, test, and deploy V2X technologies and their applications to improve transportation safety, mobility, equity, and sustainability, with ambitious short-term, medium-term, and long-term goals. These systems utilize the data generated by various interacting entities (e.g., cars, pedestrians, and cloud servers) to leverage advanced machine/deep learning and computer vision algorithms towards objectives like accident prediction and avoidance, traffic violation detection, and other safety measures. For instance, in the context of crash risk prediction, Shah et al. [25] employ a multivariate Long Short-Term Memory (LSTM) model to predict the likelihood of a crash between two V2X-enabled vehicles within the next 3 seconds, using data from the previous 7 seconds. It improves predictive capability by incorporating multiple real-time data streams, including cardinal position, acceleration, and speed transmitted by the vehicles.

Similarly, traffic violations such as red light running are often addressed through advanced object detection frameworks, including YOLO, Faster R-CNN, and SSD [5, 27]. These algorithms enable real-time detection and alert mechanisms, ensuring timely interventions. Furthermore, many V2X systems involve infrastructure-to-cloud (I2C) communication, where a third-party server (aka. a mediating agent) handles the computationally intensive deep learning operations required for accurate predictions and detections. This interplay between local and cloud-based computations exemplifies the growing integration of intelligent algorithms in real-world infrastructure, paving the way for safer and more efficient transportation ecosystems. Furthermore, driver drowsiness detection, another safety critical V2X application, also incorporates machine learning on V2X data in a distributed setting. For instance, researchers have used linear regression and convolutional neural networks to identify drowsiness in drivers over a sustained driving task [9, 2]. When in-vehicle computing resources are limited or the drowsiness detection model is proprietary, inference may be offloaded to a remote edge server.

Despite their advantages, these inference services require users to disclose their private information, such as driving speeds, electroencephalography (EEG) data, user location, license plate details, and other sensitive data points. Additionally, infrastructure that communicates with third-party servers for inference raises similar

[1] Code is available at https://github.com/datasec-lab/securev2x.

Conference'17, Washington, DC, USA

ACM ISBN 978-x-xxxx-xxxx-x/YYYY/MM
https://doi.org/10.1145/nnnnnnn.nnnnnnn

concerns regarding user data privacy. As a result, the National Deployment Plan of USDOT identified privacy protection as one of their key considerations when testing and deploying V2X technologies and applications [21]. Privacy-preserving solutions for V2X techniques require supporting fully functional V2X algorithm computations without leaking users' private data. Secure multi-party computation (MPC) offers a promising solution to address V2X privacy challenges. Especially in cases where local computation is restricted by the proprietary nature of third-party V2X machine learning algorithms, MPC allows for remote inference while providing user privacy guarantees. Several studies, such as those by Agarwal et al. [2] and Bi et al. [5], have explored secure computation applications in V2X contexts, including drowsiness detection and object detection for autonomous driving. Agarwal et al. [2] investigate secure distributed training of linear regression across multiple parties for predicting a drowsiness index, while Bi et al. [5] and Zhou et al. [31] secure the FasterRCNN and YOLOv3. Despite these advances, the high computational costs of these designs limit their practical, real-time applicability.

In this work, we focus on introducing advanced and novel MPC techniques to speed up MPC-based V2X applications. We study two representative V2X applications: (1) driver drowsiness detection, and (2) red-light violation detection (based on object detection). Models integrated for prior privacy-preserving drowsiness detection systems have included linear regression, polynomial regression, and support vector machines (for EEG data analysis and drowsiness detection) [2, 23, 19, 5]. While they have achieved reasonable performance, convolutional networks have demonstrated superior results in drowsiness detection.

Prior works on privacy-preserving object detection have explored the use of Faster-RCNN and YOLOv3. We follow the advances on object detection and design a MPC-based solution for the YOLOv5 object detector. Previous studies demonstrate that YOLOv5 achieves inference speeds approximately 10 times faster than Faster-RCNN, which is crucial for latency-sensitive applications, and may also brings efficiency improvement in the MPC setting. Furthermore, YOLOv5 maintains sufficient average bounding box precision and object classification accuracy for a range of use cases [29, 3, 15, 20]. It also offers enhanced flexibility for practitioners by providing multiple model sizes, allowing for the tuning of accuracy and inference speed to suit specific tasks.

Ensuring privacy for YOLOv5 presents additional challenges. Specifically, designing MPC solutions for all five versions of the YOLOv5 model requires the design of a unique and extremely detailed protocol for each. Moreover, YOLOv5's use of swish (*sigmoid linear unit*) activations – which help it achieve better accuracy and precision in the plaintext setting [30] – requires more complex design compared to LeakyReLU which was used in YOLOv3 [31], and ReLU in Faster-RCNN [5].

Existing MPC-based machine learning libraries provide secure protocols for a wide range of functions, but they cannot perform inference on models for V2X applications. In particular, frameworks such as Delphi, Gazelle, and CrypTFlow2 provide only the most fundamental primitives, such as secure convolutions, fully connected layers, argmax, maxpooling, and ReLU. While CrypTen offers a broader range of secure functionalities, it remains limited in flexibility. This constraint prevents most machine learning practitioners from seamlessly integrating secure computation into their workflows. To address this gap, we propose novel secure functionalities for missing operations including secure upsampling, split, and constant floor. Additionally architectural modifications are made to ensure compatibility with secure drowsiness detection.

Moreover, we revise CrypTen's underlying network graph processor to support empty-argument ONNX functions. This This drastically increases the number of V2X and machine learning applications for which downstream application is immediately accessible. Although this paper focuses on driver drowsiness and red light violation detection, the enhanced flexibility of SecureV2X compared to prior works ensures that it can easily be extended to problems such as real-time traffic flow analysis, accident prediction, and pedestrian safety. Furthermore, the behavior and complexity of operations in plaintext settings differ significantly from those in secure computation, making the selection of appropriate secure primitives and parameters for our models a complex task. We address this challenge through extensive analysis of secure primitives and hyperparameters, evaluating their impact on overall performance.

Thus, our contributions are summarized as follows:

- To our best knowledge, we propose the first real-time privacy preserving system SecureV2X for two practical V2X applications: (1) EEG-based driver drowsiness detection, and (2) red-light violation detection via YOLOv5.
- We design and implement the privacy-preserving system SecureV2X with novel cryptographic protocol constructions, which offers provable security.
- SecureV2X significantly outperforms the state-of-the-art systems for privately detecting drowsiness and red-light violation in intelligent transportation systems.

2 SecureV2X Framework

2.1 V2X Applications

Drowsiness Detection. Various methods exist for computing drowsiness detection [24]. The state-of-the-art solution relies specifically on single-channel EEG data which has been shown to be highly predictive in distinguishing between drowsy and alert driving states, as discussed in [9].

To perform drowsiness detections over an input EEG signal, we adopt the CompactCNN model [9] and its corresponding data preprocessing approach. Specifically, preprocessed EEG signals (filtered by a 1-Hz high-pass and 50-Hz low pass finite impulse response filter with muscular and ocular artifacts removed from the signal) are down-sampled from 500 Hz to 128 Hz and extracted as 3-second samples. A single channel of the EEG sample is then selected, resulting in an input vector $x \in R^{1\times 384}$. CompactCNN utilizes data sourced from a series of multi-channel EEG recordings during a "sustained-attention driving task" and uses local reaction time (the time between when a car would begin to drift, and when the driver would respond) and global reaction time (the average reaction time over trials within a 90-second window before the onset of the deviation) to measure levels of instantaneous drowsiness, accounting for baseline differences in driver reaction time [17]. If reaction times were greater than 2.5 times the baseline, the driver

was considered to be drowsy, whereas reaction times shorter than 1.5 times the baseline were labeled as "alert".

CompactCNN consists of a shallow network architecture. Namely, a single convolution layer of 32 filters of size 1 x 64 is followed by batch normalization which helps to minimize covariate shift and accelerate training convergence [9]. The ELU activation function is applied over this output to capture non-linear patterns in the data. These operations generate 32 (1×321) feature maps:

$$\text{Conv}(O_i, W_{i,\ell}, b_{i,\ell})_k = \sum_{j=1}^{64} x_{k+j} \cdot W_{i,j,\ell}, k \in [1, n]$$

$$O_{i+1} = \text{ELU}(\text{Batch}(\text{Conv}(O_i, W_{i,\ell}, b_{i,\ell})_{1\times n}))$$

$$= \text{ELU}\left(\gamma \frac{\text{Conv}(\cdot)_{1\times n} - \mu}{\sigma} + \beta \frac{\text{Conv}(\cdot)_{1\times n} - \mu}{\sigma}\right)$$

Here, ELU represents the exponential linear unit, γ and β indicate batch normalization weights and biases, μ and σ are the aggregated mean and standard deviation for the feature map output by $\text{Conv}(\cdot)$ over the training data, and $O_i, W_{i,\ell}$ and $b_{i,\ell}$ are the input tensor and filter weights and biases (for the ℓ-th filter) of the i-th layer. Global average pooling is conducted on the activation output, and a dense layer generates the final output from the pooled feature vector (1 x 32) to obtain an output of shape 1 x 2. This is passed through the log-softmax function to obtain a binary classification with regards to drowsiness. So for our final detection, we obtain

$$O_{i+2} = \text{GAP}(O_{i+1}) \cdot W_{i+1} \tag{1}$$

$$detection = \log\left(\frac{e^{O_{i+2}[1]}}{\sum_{s=0}^{1} e^{O_{i+2}[s]}}\right) \tag{2}$$

Red-Light Violation Detection via YOLOv5. Red-light violation detection is a critical area of research in traffic management. When vehicles fail to comply with traffic signals, the consequences can include property damage, injuries, and fatalities [7, 1, 26]. Additionally, red light violation detection serves as a valuable application of V2X data. To detect red light violations from video feed data, we utilize the detection algorithm proposed by [28]. First, standard image processing techniques including gray-scale binary thresholding, dilation and erosion are used to identify the detection line. A series of contours are generated and the noisy contours are filtered out. This leaves behind the crosswalk's contour components. These contours are used to generate the violation detection line. Vehicles detected beyond this point in the video feed are determined to be violators.

Second, an initial object detection is performed over the first frame. Each of these objects is assigned to a median Flow tracker [14] and tracker positions are updated every frame. For every fifth frame, an object detector scans the input to identify new vehicles in the scene and improve the precision of tracking coordinates for vehicles which are already have a tracker. These object detections are conducted by the YOLO algorithm. YOLO is a widely used machine learning algorithm in computer vision, optimized for efficiently detecting bounding boxes for objects in images.

In the original approach by Yahya et al. [28], YOLOv3 was used for this purpose. However, our system leverages the YOLOv5 model by Ultralytics. YOLOv5 comprises three main components: the backbone, neck, and detection head. The backbone extracts low-level image features, while the neck aggregates information from various depths of the backbone, forming a hierarchical feature structure that enhances detection accuracy. The detection head then generates the final bounding box predictions.

In addition to object tracking and detection, a color histogram is used to determine the color of the traffic light at any given frame. If the color is red, and a tracked vehicle's center coordinate is determined to be beyond the violation line at that point, then it is considered a red light violation.

2.2 SecureV2X Framework

Figure 1 shows that SecureV2X facilitates the secure and efficient computation of drowsiness and red-light violation detection. An edge server hosts proprietary weights for the YOLOv5n and CompactCNN models, while a connected vehicle or traffic camera (user/client) provides EEG signal data or traffic video data. Both parties engage in a secure computation protocol to jointly generate the desired output.

CryptoDrowsy performs drowsiness detection by establishing a secure communication channel between the vehicle and the edge server hosting the model. Secret shares are generated for the vehicle's EEG signal and the server's model weights. A secure mediating agent then distributes Beaver's triples for multiplications, enabling inference. Once inference is complete, the server sends its share of the output to the vehicle, which reconstructs the result. Further details on this can be found in Section 3.1.

For red-light violation detection, vehicles at or approaching an intersection connect to a traffic camera. The camera runs the detection algorithm locally, except for object detection which requires a secure connection to a model-hosting edge server. Using a secure mediating agent, the server and camera exchange random multiplicative triples to jointly compute bounding boxes over video frames. After computation, the server sends its share of the output to the camera, which reconstructs the results and applies non-maximum suppression to refine bounding boxes. If a violation is detected, the camera alerts the offending vehicle. A visual overview of this system can be seen in Figure 1.

3 Crypto-Drowsy

3.1 Secure Construction for the System

The problem of privately detecting driver drowsiness over a user (driver - Party P_0) and the service/model provider (Party P_1) is formulated as follows. P_0 holds an EEG sample vector $x \in R^{m\times n}$, and P_1 holds weights $W = \{w_1, w_2, \ldots, w_n\}$ for the EEG signal classification model. P_0 and P_1 jointly compute the classification of x, denoted as $c \in \{0, 1\}$, where 0 indicates a negative classification (the driver is not drowsy) and 1 indicates a positive classification (the driver is drowsy). During the classification procedure, we require that P_0 learns nothing about P_1's model (the proprietary pretrained weights of a publicly known architecture) except for its inference output, and P_1 obtains no information about P_0's input data and its inference output.

To maintain the privacy of pretrained model weights (held by the service provider) and input data (held by the user), we design a specific secure protocol for driver drowsiness detection, and utilize the CrypTen MPC framework [16] for the concrete implementation.

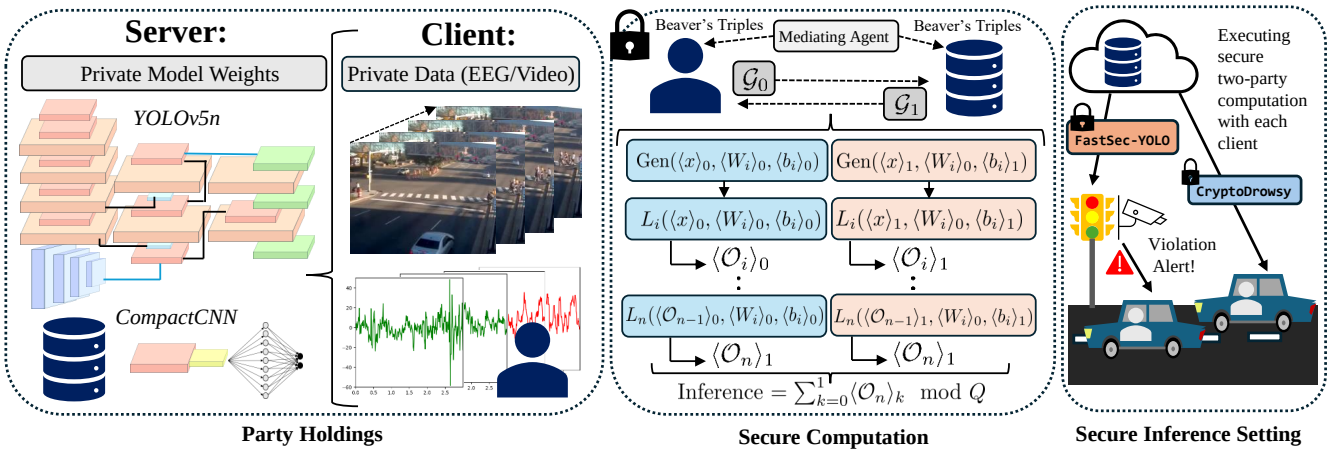

Figure 1: Overview for the SecureV2X Framework. Server: edge server or the cloud (infrastructure), Client: connected vehicle and/or traffic camera. The server is executing secure two-party computation with each client.

Algorithm 1 CryptoDrowsy

Input: P_0 holds EEG sample $x \in \mathbb{R}^{1\times 384}$ and P_1 holds model weights $W = \{W_1, W_2, W_3\}$ and biases $b = \{b_1, b_2, b_3\}$
Output: P_0 learns drowsiness classification, $c \in \{0, 1\}$

1: P_k for parties $k \in \{0, 1\}$ invoke $\mathcal{F}_{PRZS}$ to generate secret shares of their inputs, $\langle x\rangle_k, \langle W_i\rangle_k, \langle b_i\rangle_k$, where $i \in \{1, 2, 3\}$
2: P_k for parties $k \in \{0, 1\}$ invoke $\mathcal{F}_{Conv2D}$ and provide input shares $\langle x\rangle_k, \langle W_1\rangle_k, \langle b_1\rangle_k$ and obtain $\langle O_1\rangle_k$
3: P_k for parties $k \in \{0, 1\}$ call $\mathcal{F}_{BN}$ on shares $\langle O_1\rangle_k, \langle W_2\rangle_k, \langle b_2\rangle_k$ to obtain $\langle O_2\rangle_k$
4: P_k for parties $k \in \{0, 1\}$ call $\mathcal{F}_{ReLU}$ and input shares $\langle O_2\rangle_k$ and learn $\langle O_2'\rangle_k$
5: P_k for parties $k \in \{0, 1\}$ reshape shares $\langle O_2'\rangle_k$ to $1 \times 32 \times 321$ and perform global pooling for each 1×321 feature map to output $\langle O_2''\rangle_k$ of shape 1×32
6: P_k for parties $k \in \{0, 1\}$ input $\langle O_2''\rangle_k$, $\langle W_3\rangle_k$ and $\langle b_3\rangle_k$ to $\mathcal{F}_{FC}$ and output $\langle O_3\rangle_k$
7: P_1 sends its output share $\langle O_3\rangle_1$ to P_0 who reconstructs $c = \langle O_3\rangle_0 + \langle O_3\rangle_1$

Algorithm 1 shows the detailed protocol description. Here, we show its design idea. Under the CrypTen framework, P_0 or P_1 holds secret shares of the other party's inputs (the EEG sample and model weights owned by the user and the service provider, respectively). To share an input x, a pseudorandom zero-share (PRZS) [8] is first generated by P_0 and P_1 that sum to 0. Then, the party that holds the input x adds x to their share and discards x. For ease of description, in the rest of the paper, we denote $\langle x\rangle$ as the shares of x, and $\langle x\rangle_0, \langle x\rangle_1$ as the shares of x owned by P_0 and P_1, respectively. All computations f involved for the inference done by CrypTen follows the paradigm that P_0 and P_1 own $\langle f(x)\rangle$. Therefore, it is easy to reveal the final inference result, that is, the service provider P_1 sends its output share to the user P_0 so that the user obtains its inference result as the sum of the resulting shares.

Additive shares have homomorphic properties, which allow for private addition, multiplication, comparison, and other non-linear computations. Given two shares $\langle x\rangle$, $\langle y\rangle$, private addition can be easily done by having P_0 and P_1 compute $\langle z\rangle_i = \langle x\rangle_i + \langle y\rangle_i$ for $i \in \{0, 1\}$, respectively. Multiplication of a public value p and a share $\langle x\rangle$ can be also easily done by having P_0 and P_1 compute $\langle z\rangle_i = p \cdot \langle x\rangle_i$. Private multiplication is non-trivial. CrypTen introduces a helper party T to assist with private multiplication by generating Beaver triples [4] $(\langle a\rangle, \langle b\rangle, \langle c\rangle)$ where $c = ab$. With the help of the Beaver triple, P_0 and P_1 compute $\langle e\rangle = \langle x\rangle - \langle a\rangle$ and $\langle d\rangle = \langle y\rangle - \langle b\rangle$, and reveal the output to obtain public values e and d. This enables the computation of $\langle x\rangle\langle y\rangle = \langle c\rangle + e\langle b\rangle + \langle a\rangle d + ed$. Private comparison between $\langle x\rangle$ and $\langle y\rangle$ extracts the highest shared bit of the subtraction of $\langle x - y\rangle$, which can be efficiently done via a special MPC protocol B2A [12]. Additional details about these conversions are provided in Appendix 5.2.

We now detail the computations involved in CompactCNN. Input shares are first generated, and Beaver triples are distributed by the helper to compute the initial convolution. Batch normalization is applied to the resulting arithmetic shares using CrypTen's summation, public division, and variance functions. ReLU activation employs a multiplexer to compute $\langle x > 0\rangle$, setting $\langle 1\rangle$ if $x > 0$ or $\langle 0\rangle$ otherwise. ReLU is then calculated as $\langle x\rangle\langle x > 0\rangle$.

Global average pooling computes the mean across the 1×321 feature map by summing the secret-shared tensor and performing public division to avoid fixed-point encoding errors (see CrypTen [16]). The dense layer leverages Beaver triples for secure matrix multiplication between the weights tensor and the input. The network's output is finalized using CrypTen's approximations for the log-softmax function, applied directly to secret-shared data via Newton-Raphson iterations for exponentiation and maximum/summation protocols.

All functions rely on CrypTen's secure multiparty computation primitives. Once computation is complete, the server sends its share of the result to the user, who combines it with their own and scales down to reconstruct the plaintext output. The security of these operations within CryptoDrowsy is discussed in section 5.

4 FastSec-YOLO

4.1 Secure Construction for the System

As explained in section 2.2, we do not implement the entire RLR detection algorithm in a private context. Instead, we leverage CrypTen to convert YOLOv5 to a CrypTensor-based network, enabling the generation of secret shares for both the provider's model and the user's data. In this setup, most components of the algorithm are computed locally, with only object detection performed via secure two-party computation.

CrypTen seamlessly converts most PyTorch models into its framework, thanks to its extensive library of secure functions. However, key components of the YOLOv5 architecture, such as upsampling and tensor splitting, were not originally supported. To address this, we developed customized secure protocols for these operations, enabling the use of YOLOv5 for secure object detection. A detailed description of the protocol can be found in Algorithm 2.

As with CryptoDrowsy, FastSec-YOLO enables a client (Party P_0) and a model provider (Party P_1) over secretly shared input data and model weights owned by P_0 and P_1, respectively. Here, P_0 holds a square image $x \in \mathbb{R}^{m \times m \times 3}$ where m is some multiple of 32, and P_1 holds weights $W = \{w_1, w_2, \ldots, w_n\}$ for the trained YOLOv5n object detector. Together, P_0 and P_1 compute a detection output of shape $O \in \mathbb{R}^{n \times 85}$ where n is the number of detections made, and the first five columns correspond to the object class, x and y center values, the width, and the height of the output bounding box, respectively. The other 80 columns indicate the confidence estimate for each possible detection class.

Here, we present the protocol design for FastSec-YOLO. Additional details about its construction can be seen in figure 2. As with CryptoDrowsy, computation starts with the generation of secret shares through the PRZS algorithm, and the distribution of Beaver's triples involved in the convolutions performed over YOLOv5n. The semantics of these procedures are identical to those involved in computing CryptoDrowsy and can be referred to in Section 3.1.

FastSec-YOLO's computation involves three core components: the backbone, the neck, and the detection head. First, the CSPDarknet backbone of YOLOv5n computes feature maps from the input image, with cross-stage connections facilitating the flow of information from lower network levels to the feature aggregation neck. Next, the PANet neck aggregates these features and passes them to the detection head, which outputs bounding box detections, classifications, and confidence estimates for each class. Each network component utilizes C3 convolution blocks, incorporating convolution, batch normalization, and Swish activation functions. The secure protocol for computing these blocks is detailed in Algorithm 4 in the appendix. At the backbone's end, spatial pyramid pooling extracts the network's most critical features, with the secure implementation described in Algorithm 7 in the Appendix. Finally, the aggregation neck applies secure upsampling and further convolution operations to enhance bounding box detection accuracy, particularly for small objects.

After the forward pass of FastSec-YOLO, the model holder sends its output shares to the data holder. In this scheme, both parties must agree on how the shares are redistributed, ensuring that the server cannot access the user's output data— which is inherently sensitive—without permission. Under the semi-honest model assumption, the protocol dictates that the server sends its shares to the user, while the user does not return its own shares to the server. The user then sums and scales its shares to reconstruct the final output bounding boxes. The underlying security of SecureV2X – and by extension FastSec-YOLO and CryptoDrowsy – is discussed further in section 5.

Algorithm 2 FastSec-YOLO

Input: P_0 holds normalized image $x \in \mathbb{R}^{k \times l \times 3}$ and P_1 holds weight sets $W = \{W_1, W_2, \ldots, W_n\}$ and bias sets $b = \{b_1, b_2, \ldots, b_n\}$
Output: P_0 learns output $z \in \mathbb{R}^{m \times 85}$ where m is the number of raw bounding boxes generated

Parties $P_k, k \in \{0, 1\}$ invoke $\mathcal{F}_{PRZS}$ to obtain secret shares of x, W, and b, $\langle x \rangle_k, \langle W_i \rangle_k, \langle b_i \rangle_k$ for all $i \in \{1, 2, \ldots, n\}$
Initialize dictionary *ResWeights*
For $k \in \{0, 1\}$, $\langle O_0 \rangle_k \leftarrow \langle x \rangle_k$
for $i = 1, 2, \ldots, n$ **do**
    if L_i = ConvBNSiLU **then**
        $\langle O_i \rangle_k \leftarrow \mathcal{F}_{ConvBNSiLU}(\langle O_{i-1} \rangle_k, \langle W_i \rangle_k, \langle b_i \rangle_k)$
        if ConvBNSiLU has residual connection **then**
            $ResWeights[i] = \langle O_i \rangle_k$
    else if L_i = Conv2D **then**
        $\langle O_i \rangle_k \leftarrow \mathcal{F}_{Conv2D}(\langle O_{i-1} \rangle_k, \langle W_i \rangle_k, \langle b_i \rangle_k)$
        if Conv2D has residual connection **then**
            $ResWeights[i] = \langle O_i \rangle_k$
    else if L_i = C3 **then**
        $\langle O_i \rangle_k \leftarrow \mathcal{F}_{C3}(\langle O_{i-1} \rangle_k, \langle W_i \rangle_k, \langle b_i \rangle_k)$
        if C3 has residual connection **then**
            $ResWeights[i] = \langle O_i \rangle_k$
    else if L_i = SPPF **then**
        $\langle O_i \rangle_k \leftarrow \mathcal{F}_{SPPF}(\langle O_{i-1} \rangle_k, \langle W_i \rangle_k, \langle b_i \rangle_k)$
    else if L_i = Concat (ℓ) **then**
        $\langle O_i \rangle_k \leftarrow \mathcal{F}_{Concat}(\langle O_{i-1} \rangle_k, ResWeights[\ell])$
    else if L_i = Upsample **then**
        $\langle O_i \rangle_k \leftarrow \mathcal{F}_{Upsample}(\langle O_{i-1} \rangle_k)$
P_1 sends its share $\langle O_n \rangle_k$ to P_0 who reconstructs the output z from its shares

5 Security of SecureV2X

SecureV2X is composed of CryptoDrowsy and FastSec-YOLO, each implementing functionalities for computing convolutions, batch normalization, max pooling, sigmoid linear unit activations, ReLU activations, global pooling, fully connected layers, concatenation, and upsampling. These functionalities rely on combinations of primitive operations, including addition, multiplication, comparison, and public division. Non-linear functions, such as the inverse square root (used in batch normalization) and the sigmoid, are implemented using linear approximations based on these primitive operations.

Both CryptoDrowsy and FastSec-YOLO rely on the secure primitives provided by CrypTen [16]. All secure functions implemented by CrypTen involve arithmetic and binary secret-sharing, and conversions between the two for efficiency. As demonstrated in [11], the security of functions is preserved under composition. Therefore, the security of our system and all involved functions is derived from the security of the compositions of these secure primitives.

Tensor operations such as concatenation, upsampling, and splitting are non-interactive, meaning they can be performed locally on secret-shared data. Thus, their security trivially follows from the security of the secret-sharing paradigm in use. Addition operations performed over arithmetic secret shares are also non-interactive, which means that they are trivially secure as well. All secure multiplication and addition operations are performed over arithmetic secret shares in the ring $\mathbb{Z}_{2^L}$, which have been proven secure in [6, 16].

5.1 Secure Operations over Binary Secret Shares

Secure comparison underlies the secure activation functions provided by the CrypTen framework. These operations are performed over binary secret shares, which are more efficient for this task. Additionally, logic and multiplexing operations involved in max pooling, an essential component of the spatial pyramid pooling block in YOLOv5's architecture, are performed over binary secret shares. Operations conducted over binary secret shares are represented as Boolean circuits using the GMW protocol [13]. Three fundamental logic operators are defined in this setting.

First, `XOR` can be computed locally on each party's secret shares. Suppose $\langle z\rangle^B = \langle x\rangle^B \oplus \langle y\rangle^B$. Then, P_i locally computes $\langle z\rangle_i^B = \langle x\rangle_i^B \oplus \langle y\rangle_i^B$. Since this protocol involves no communication, the operation is non-interactive and secure.

Second, `AND` operations are computed over these shares. For $\langle z\rangle^B = \langle x\rangle^B \wedge \langle y\rangle^B$, a precomputed Boolean triple $\langle c\rangle^B = \langle a\rangle^B \wedge \langle b\rangle^B$, where a and b consist of bits sampled uniformly at random, is used to compute the output since bitwise `AND` is equivalent to multiplication modulo 2. As described in [12], P_i obtains $\langle e\rangle^B = \langle a\rangle_i^B \oplus \langle x\rangle_i^B$ and $\langle f\rangle_i^B = \langle b\rangle_i^B \oplus \langle y\rangle_i^B$. Each party then reconstructs e and f by exchanging their respective shares, $\langle e\rangle_i^B$ and $\langle f\rangle_i^B$, and computing the `XOR` of the received shares. Since a and b are sampled at random, the values of e and f reveal no information about x or y. Finally, P_i computes $i \cdot e \cdot f \oplus f \cdot \langle a\rangle_i^B \oplus e \cdot \langle b\rangle_i^B \oplus \langle c\rangle_i^B = \langle z\rangle_i^B$.

Lastly, `Bit-Shift` operations can be efficiently computed over binary secret shares. When parties wish to shift the bits of a binary secret-shared value $\langle x\rangle^B$ by a constant k, each party locally computes $\langle y\rangle_k^B = \langle x\rangle_k^B >> k$. Since each bit of a binary secret-shared value is independent of all other secret-shared bits, bit shifts can be easily performed over binary secret shares. The non-interactivity of this operation ensures its security.

5.2 A2B and B2A Secret Share Conversions

Because some operations are more efficiently computed over arithmetic secret shares and others over binary secret shares, it is important to use efficient conversions between the two types. CrypTen's primitives for computing max pooling, ReLU, and other functionalities convert input arithmetic secret shares to binary secret shares, compute the logical function, and then convert the output back into arithmetic secret shares.

The security of arithmetic-to-binary (A2B) secret share conversions is demonstrated in [10]. Each party secretly transmits its arithmetic share to the other and then performs addition over both shares. Next, both parties instantiate binary secret shares $\langle y\rangle_k^B$, where each y_k is an arithmetic secret share, i.e., $y_k = \langle x\rangle_k$. Once these secret shares are defined, each party computes $\langle x\rangle = \sum_{k\in\mathcal{P}} \langle y\rangle_k^B$. CrypTen's primitives employ two approaches to compute this sum. If memory is sufficient, a carry-lookahead adder circuit is used to evaluate the sum in $\log_2(|\mathcal{P}|)\log_2(L)$ rounds. However, if GPU memory is exceeded, a less memory-demanding protocol is adopted, which requires $|\mathcal{P}|\log_2(L)$ rounds to compute.

Converting binary shares to arithmetic shares (B2A) is accomplished as follows. First, parties compute $\langle x\rangle = \sum_{b=1}^{B} 2^b \langle\langle x\rangle^{(b)}\rangle$, where $\langle x\rangle^{(b)}$ indicates the b-th bit of the binary share $\langle x\rangle^B$ (B is the total number of bits in the secret being shared). The arithmetic shares of bits are created using B pairs of secret-shared bits $(\langle r\rangle, \langle r\rangle^B)$ during the offline phase. Each pair represents the bit-value r in both arithmetic and binary secret-share forms. Next, each party computes $\langle z\rangle^B \leftarrow \langle b\rangle^B \oplus \langle r\rangle^B$. This result is revealed and used to compute $\langle b\rangle \leftarrow \langle r\rangle + z - 2\langle r\rangle z$. In this scheme, the secret shares $\langle r\rangle^B$ are chosen uniformly at random. Consequently, the revealed value $\langle z\rangle^B \leftarrow \langle b\rangle^B \oplus \langle r\rangle^B$ is *indistinguishable from white Bernoulli random noise.* This ensures the security of the conversion. For more detailed proof of this, see §C.1.3 in [16].

6 Experimental Results

For both CryptoDrowsy and FastSec-YOLO, we evaluate performance using three key metrics: accuracy, communication, and efficiency. Secure computations rely on fixed-point representations instead of high-precision floating-point values used in plaintext settings, leading to minor performance degradations in privacy-preserving machine learning. Additionally, certain secure operations require approximations for efficiency, further impacting accuracy. Measuring the extent of these degradations across different secure systems is crucial. The main obstacle to the widespread adoption of secure computation protocols in machine learning and V2X settings is their inefficiency compared to plaintext counterparts. Therefore, our evaluation primarily focuses on how efficiently these computations can be performed under various parameters and configurations.

6.1 Secure Drowsiness Detection

The plaintext drowsiness detector (CompactCNN) achieves an accuracy of 0.8184 while the Delphi-based secure system performs slightly worse, at 0.7675. On the other hand, CrypTen and CrypTFlow2 achieve exactly the same results as the plaintext model, with accuracy scores of 0.8184 for each. The F1-Scores reflect this as well. CrypTen and CrypTFlow2 achieve the same results in plaintext at 0.8394, while Delphi's system results in an F1-score of 0.8064.

This discrepancy may be related to the use of homomorphic encryption and numerical approximations in Delphi which help to achieve a higher level of security but reduces the accuracy of the system overall. In contrast, CrypTFlow2 and CrypTen use precise secret sharing schemes which enable more accurate computations. Moreover, CrypTFlow2 and CrypTen achieve better runtime performance by foregoing the expensive preprocessing computations required for homomorphic encryption schemes in favor of relatively cheap oblivious transfers in the case of CrypTflow2, and the use of a secure mediating agent in the case of CrypTen.

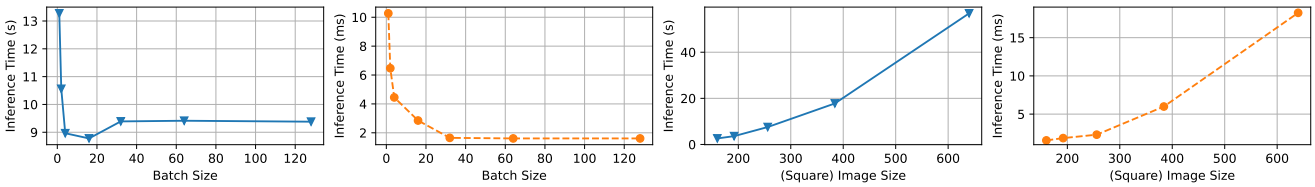

(a) Secure Inf. by Batch Size **(b) Plain Inf. by Batch Size** **(c) Secure Inf. by Image Size** **(d) Plain Inf. by Image Size**

Figure 2: Evaluation of FastSec-YOLO on Varying Batch and Image Sizes under the Secure and Plaintext Settings. We compute object detection for batch sizes of 1, 2, 4, 16, 32, 64 and image resolutions of 160×160, 192×192, 256×256, 384×384 and 640×640.

Table 1: MAP50, Mean Precision (MP), Mean Recall (MR), Communication Cost, and Runtime (efficiency) metrics for each private object detection system over vehicle classes. All systems, have the same fixed parameters (batch size is 32, image size is 288×288).

System	MAP50	MR	CPU Time (s)	GPU Time (s)	Com. (MB)	Rounds
Fast Sec-YOLO	0.4388	0.3425	8.7781	1.734	151.5	77.5
CrypTen-YOLOv5s	0.4563	0.3678	19.2428	3.593	288.0	77.5
CrypTen-YOLOv5m	0.6162	0.5241	36.9849	8.000	497.2	102.5
CrypTen-YOLOv5l	0.6918	0.6136	59.8448	14.292	755	127.5
CrypTen-YOLOv5x	0.7549	0.6460	97.0974	26.017	1,061.5	152.5

Table 2: Average runtime, communication, and round complexity performance on private drowsiness detection (our CryptoDrowsy vs. relevant benchmarks for a batch of 314 EEG signals).

System	CPU Time (s)	Com. (MB)	Rounds
DelphiDrowsy	92.961	277.085	-
CrypTFlowDrowsy	0.254	87.496	59
CryptoDrowsy	0.027	5.271	0.411

6.2 Private Red-Light Running Detection

We evaluate the performance of our privacy-preserving red light violation detection system by studying its underlying object detector in two ways. First, we compare the performance of our chosen private object detector, FastSec-YOLO, across a series of different image resolutions and batch sizes. For image and batch size, we report variations in the running time performance of the system. In addition, we analyze the detection accuracy and speed of our Fast-SecYOLO compared to alternative secure YOLOv5 systems. Second, we compare the efficiency of our chosen private system against the relevant secure benchmarks, including Faster-RCNN [5, 19] and YOLOv3-SPP [31].

When running YOLOv5 in plaintext or secure settings, batch size and image size can be adjusted to balance inference speed and accuracy. In both settings, increasing the image size results in a monotonic increase in inference time, as shown in Figures 2d and 2c. However, larger image sizes also improve inference accuracy. Based on an empirical analysis of detection outcomes with FastSec-YOLO, an image size of 288×288 was found to be optimal, offering the best trade-off between inference speed and accuracy for red light violation detection. Batch size, on the other hand, affects only inference speed. The optimal batch size is 16, as larger sizes slightly increase inference time. Performance does not degrade beyond a batch size of 32. This contrasts with plaintext YOLOv5, where inference time decreases monotonically with increasing batch size, stabilizing beyond a batch size of 32.

Table 1 summarizes the average CPU and GPU inference times, average precision for relevant RLR vehicle classes (1, 2, 3, 5, and 7), communication overhead, and communication rounds per image across batches of 32 images resized to 288×288. These results are based on the COCO128 baseline dataset, a subset of COCO [18], used to train and evaluate the YOLOv5 object detector. FastSec-YOLO demonstrates significantly better runtime performance, requiring nearly 90 seconds less than CrypTen-YOLOv5x on the CPU and 25 seconds less on the GPU. However, this comes with a tradeoff: FastSec-YOLO, built on YOLOv5n—the smallest YOLOv5 model—shows notably lower average precision compared to CrypTen-YOLOv5x. This tradeoff may be acceptable for some instances, such as red light violation detection, where higher resolution vehicle classifications require only moderate precision. The plaintext RLR detection algorithm proposed by [28], based on YOLOv3, achieves an F1-score of 0.93 for identifying violators. Since FastSec-YOLO achieves precision comparable to YOLOv5s (equivalent to YOLOv3), our secure RLR detection system has similar performance as the plaintext version.

Table 3: Average runtime, communication, and round complexity performance compared between our system, FastSec-YOLO and relevant benchmarks as reported.

System	Model	Time (s)	Com. (MB)
FastSec-YOLO	YOLOv5n	**1.734**	151.5
SecRCNN [19]	FasterRCNN	180	150
P2OD [5]	FasterRCNN	190.527	6166.723
PPDF [31]	YOLOv3-SPP	276	163.1

Table 3 compares the inference speed of FastSec-YOLO with other private object detectors as reported.[2] This comparison demonstrates

[2]For prior works without open-sourced code, we included their reported results for comparison.

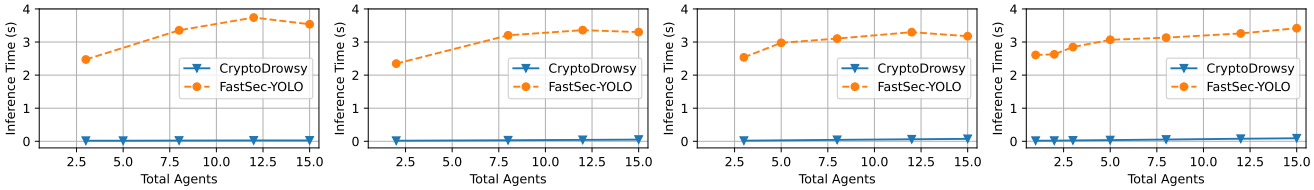

(a) 25% Split Agent Types (b) 50% Split Agent Types (c) 75% Split Agent Types (d) 100% Single Agent Type

Figure 3: Evaluation of SecureV2X on Simultaneously Supporting Multiple Vehicles (in different ratios). Each subfigure displays the reported inference times when instances of CryptoDrowsy or FastSec-YOLO represent a given percentage of the systems (clients) being run. We conduct the evaluations by setting a total number of secure processes ranging from 1 to 15 at once.

Table 4: MAP50, Mean Precision (MP), Mean Recall (MR) and Runtime (efficiency) metrics for each of the models in a plaintext setting. Mean precision and recall account for all classes. Batch size: 32, and input resolution: 288 × 288.

Model	MAP50	MP	MR	Time (s)
YOLOv5n	0.4388	0.4939	0.3425	0.0027
YOLOv5s	0.4591	0.5425	0.3678	0.0047
YOLOv5m	0.6150	0.6584	0.5234	0.0091
YOLOv5l	0.6916	0.7618	0.6136	0.0172
YOLOv5x	0.7552	0.7837	0.6467	0.0332

the superior efficiency of our system. Whereas other secure systems all require in excess of 180 seconds to compute (as reported), FastSec-YOLO requires only 1.734 seconds. This comes far closer to real-time performance than any of the prior work.

6.3 Multi-Agent System Performance

To evaluate how the efficiency of SecureV2X is affected by increased server loads while supporting multiple agents of different types, we conduct a series of multi-agent evaluations. In each setting, the server initializes a series of CryptoDrowsy and FastSec-YOLO processes simultaneously for a certain number of total clients. For our experiments, we set the number of total clients as either 1, 2, 3, 5, 8, 12, and 15 and the proportion of agents executing either CryptoDrowsy or FastSec-YOLO to 0.00, 0.25, 0.50, 0.75, or 1.00 while the remaining agents run the opposite protocol. Each agent running CryptoDrowsy processes the same set of 314 1×384 EEG vectors whereas each instance of FastSec-YOLO processes the same batch of 4 frames - scaled to a size of 288×288 - from a real life red light violation recording.

The results are shown in Figure 3. Each subfigure illustrates the performance of CryptoDrowsy and FastSec-YOLO as their execution comprises a varying proportion of agents in the simulation. As expected, the average inference time per input increases with the number of agents. In all four sets of simulations, average inference times per agent are minimized where the total number of agents is the fewest. When more resources can be dedicated to a smaller set of agents, then their associated run times should be reduced. However, as the number of agents increases, the runtime increases only marginally. Specifically, the difference in average inference time per agent when the number of agents is 1 and 15 is at most 1 second for FastSec-YOLO (RLR Agents) and 74 milliseconds for CryptoDrowsy (Driver Agents).

7 Related Works

In EEG-based drowsiness detection, Agarwal et al. [2] proposes a secure linear regression system which makes use of secure multiparty-computation via additive secret sharing to jointly train linear regression models for predicting drowsiness states. As an alternate approach, Popsecu et al. [23] implement privacy preserving EEG signal classification through the use of homomorphic encryption. This approach preserves the correctness of linear operations over the data while maintaining its privacy.

Several studies have explored secure implementations of object detection algorithms for applications in autonomous driving, traffic violation detection, and more. Due to the depth of object detection networks, homomorphic encryption proves inefficient for these computations. Instead, works such as [31], [19], and [5] employ additive secret sharing with a trusted third party to distribute random multiplicative triples (Beaver's triples). However, these approaches are too slow for real-time applications, each requiring at least 180 seconds per inference. Conversely, Visor offers a more efficient but less secure solution [22]. This system uses a hybrid trusted execution environment (TEE) that optimizes CPU and GPU resources across vision tasks. For object detection, Visor securely implements the YOLO detector, achieving near-plaintext inference speeds. Despite its efficiency, TEEs are susceptible to side-channel attacks and other vulnerabilities that MPC can avoid.

8 Conclusion

In this work, we introduce SecureV2X, a unified framework for tackling safety- and privacy-critical challenges in V2X and intelligent transportation. We design CryptoDrowsy for fast, private drowsiness detection and FastSec-YOLO for real-time red light violation detection. SecureV2X significantly outperforms benchmark secure systems, with CryptoDrowsy achieving nearly 10× faster inference than CrypTFlow2 and FastSec-YOLO exceeding the next fastest benchmark by over 100×. These efficiency gains enable practical, time-sensitive safety applications while preserving user data privacy and proprietary model security.

Acknowledgment

This work is partially supported by the National Science Foundation (NSF) under Grants No. CNS-2302689, CNS-2308730, CNS-2319277, CNS-2432533, CMMI-2326341 and ITE-2452747, as well as by a Cisco Research Award.

References

[1] AAA. 2019. Red light running crash fatalities. (2019). https://us.vocuspr.com/Newsroom/ViewAttachment.aspx?SiteName=AAACS&Entity=PRAsset&AttachmentType=F&EntityID=110661&AttachmentID=a05c7218-b5a8-4f9e-868d-557e5959f030.

[2] Anisha Agarwal, Rafael Dowsley, Nicholas D. McKinney, Dongrui Wu, Chin-Teng Lin, Martine De Cock, and Anderson C. A. Nascimento. 2019. Protecting Privacy of Users in Brain-Computer Interface Applications. *IEEE Transactions on Neural Systems and Rehabilitation Engineering*, 27, 8, (Aug. 2019), 1546–1555. Conference Name: IEEE Transactions on Neural Systems and Rehabilitation Engineering. DOI: 10.1109/TNSRE.2019.2926965.

[3] Khaled R. Ahmed. 2021. Smart Pothole Detection Using Deep Learning Based on Dilated Convolution. *Sensors*, 21.

[4] Donald Beaver. 1991. Efficient multiparty protocols using circuit randomization. In *11th Annual International Cryptology Conference*. Springer, 420–432.

[5] Renwan Bi, Jinbo Xiong, Youliang Tian, Qi Li, and Kim-Kwang Raymond Choo. 2023. Achieving Lightweight and Privacy-Preserving Object Detection for Connected Autonomous Vehicles. *IEEE Internet of Things Journal*, 10, 3, (Feb. 2023), 2314–2329. Conference Name: IEEE Internet of Things Journal. DOI: 10.1109/JIOT.2022.3212464.

[6] Dan Bogdanov, Sven Laur, and Jan Willemson. 2008. Sharemind: a framework for fast privacy-preserving computations. In *Computer Security - ESORICS 2008*. Springer Berlin Heidelberg, 192–206.

[7] Ellen G. Cohn, Suman Kakar, Chloe Perkins, Rebecca Steinbach, and Phil Edwards. 2020. Red light camera interventions for reducing traffic violations and traffic crashes: a systematic review. *Campbell Systematic Reviews*, 16, 2, 1–52.

[8] Ronald Cramer, Ivan Damgård, and Yuval Ishai. 2005. Share conversion, pseudorandom secret-sharing and applications to secure computation. In *Theory of Cryptography: Second Theory of Cryptography Conference, TCC 2005, Cambridge, MA, USA, February 10-12, 2005. Proceedings 2*. Springer, 342–362.

[9] Jian Cui, Zirui Lan, Yisi Liu, Ruilin Li, Fan Li, Olga Sourina, and Wolfgang Müller-Wittig. 2022. A compact and interpretable convolutional neural network for cross-subject driver drowsiness detection from single-channel EEG. en. *Methods*, 202, (June 2022), 173–184. DOI: 10.1016/j.ymeth.2021.04.017.

[10] Ivan Damgård, Fitzi Matthias, Eike Kiltz, Jesper Buus Nielsen, and Tomas Toft. 2006. Unconditionally secure constant-rounds multi-party computation for equality, comparison, bits and exponentiation. In *Proceedings of the Third Conference on Theory of Cryptography*. Springer Berlin Heidelberg, 285–304.

[11] Ivan Damgård, Valerio Pastro, Nigel Smart, and Sarah Zakarias. 2012. Multiparty computation from somewhat homomorphic encryption. In *Proceedings of the 32nd Annual Cryptology Conference on Advances in Cryptology*. Springer Berlin Heidelberg, 643–662.

[12] Daniel Demmler, Thomas Schneider, and Michael Zohner. 2015. Aby - a framework for efficient mixed-protocol secure two-party computation. In *NDSS Symposium 2015*. NDSS, 1–15.

[13] Oded Goldreich, Silvio Micali, and Avi Widerson. 1987. How to play any mental game, or a completeness theorem for protocols with honest majority. In *Proceedings of the nineteenth annual ACM symposium on Theory of computing*. STOC, 218–229.

[14] Zdenek Kalal, Krystian Mikolajczyk, and Jiri Matas. 2010. Forward-Backward Error: Automatic Detection of Tracking Failures. In *2010 20th International Conference on Pattern Recognition*. IEEE, 2756–2759.

[15] Aicha Khalfaoui, Abdelmajid Badri, and Ilham EL Mourabit. 2022. Comparative Study of YOLOv3 and YOLOv5's Performances for Real-time Person Detection. In *2022 2nd International Conference on Innovative Research in Applied Science, Engineering and Technology (IRASET)*. IEEE, 1–5.

[16] Brian Knott, Shobha Venkataraman, Awni Hannun, Shubho Sengupta, Mark Ibrahim, and Laurens van der Maaten. 2022. CrypTen: Secure Multi-Party Computation Meets Machine Learning. en. arXiv:2109.00984 [cs]. (Sept. 2022). Retrieved Aug. 5, 2024 from http://arxiv.org/abs/2109.00984.

[17] Chin-Teng Lin, Ruei-Cheng Wu, Sheng-Fu Liang, Wen-Hung Chao, Yu-Jie Chen, and Tzyy-Ping Jung. 2005. Eeg-based drowsiness estimation for safety driving using independent component analysis. *IEEE Transactions on Circuits and Systems I*, 52, 12, 2726–2738.

[18] Tsung-Yi Lin et al. 2015. Microsoft coco: common objects in context. (2015). arXiv: 1405.0312 [cs.CV].

[19] Yang Liu, Zhuo Ma, Ximeng Liu, Siqi Ma, and Kui Ren. 2022. Privacy-Preserving Object Detection for Medical Images With Faster R-CNN. *IEEE Transactions on Information Forensics and Security*, 17, 69–84. Conference Name: IEEE Transactions on Information Forensics and Security. DOI: 10.1109/TIFS.2019.2946476.

[20] Upesh Nepal and Hossein Eslamiat. 2022. Comparing YOLOv3, YOLOv4, and YOLOv5 for Autonomous Landing Spot Detection in Faulty UAVs. *Sensors*, 22, 2, 1–15.

[21] US Department of Transportation. 2024. Usdot releases national deployment plan for vehicle-to-everything (v2x) technologies to reduce death and serious injuries on america's roadways. (2024). https://www.transportation.gov/briefing-room/usdot-releases-national-deployment-plan-vehicle-everything-v2x-technologies-reduce.

[22] Rishabh Poddar, Ganesh Ananthanarayanan, Srinath Setty, Stavros Volos, and Raluca Ada Popa. 2020. Visor: Privacy-Preserving video analytics as a cloud service. In *29th USENIX Security Symposium (USENIX Security 20)*. USENIX Association, (Aug. 2020), 1039–1056. ISBN: 978-1-939133-17-5. https://www.usenix.org/conference/usenixsecurity20/presentation/poddar.

[23] Andreea Bianca Popescu, Ioana Antonia Taca, Cosmin Ioan Nita, Anamaria Vizitiu, Robert Demeter, Constantin Suciu, and Lucian Mihai Itu. 2021. Privacy Preserving Classification of EEG Data Using Machine Learning and Homomorphic Encryption. en. *Applied Sciences*, 11, 16, (Jan. 2021), 7360. Number: 16 Publisher: Multidisciplinary Digital Publishing Institute. DOI: 10.3390/app11167360.

[24] Muhammad Ramzan, Hilkmat Ullah Khan, Shahid Mahmood Awan, Amina Ismail, Mahwish Ilyas, and Mahmood Ahsan. 2019. A survey on state-of-the-art drowsiness detection techniques. *IEEE Access*, 7, 61904–61919.

[25] Foram N. Shah, Dhaval K. Patel, Kashish D. Shah, Mehul S. Raval, Mukesh Zaveri, and S.N. Merchant. 2023. Novel Crash Prevention Framework for C-V2X using Deep Learning. In *2023 15th International Conference on COMmunication Systems & NETworkS (COMSNETS)*. ISSN: 2155-2509. (Jan. 2023), 7–12. DOI: 10.1109/COMSNETS56262.2023.10041397.

[26] David M Studdert, Simon J Walter, and Jeremy J Goldhaber-Fiebert. 2017. Once ticketed, twice shy? specific deterrence from road traffic laws. In *Health Law Workshops*. Harvard Law School.

[27] Le Quang Thao, Duong Duc Cuong, Nguyen Tuan Anh, Pham Mai Anh, Ha Minh Duc, and Nguyen Minh. 2022. Automatic Traffic Red-Light Violation Detection Using AI. en. *Ingénierie des systèmes d information*, 27, 1, (Feb. 2022), 75–80. DOI: 10.18280/isi.270109.

[28] Ahmad Yahya, Ihab Abdelkareem, and Osama Al-fakhouri. [n. d.] Fully-automated-red-light-violation-detection. (). https://github.com/AhmadYahya97/Fully-Automated-red-light-Violation-Detection/tree/master.

[29] Muhamad Munawarar Yusro, Rozniza Ali, and Muhammad Suzuri Hitam. 2023. Comparison of Faster R-CNN and YOLOv5 for Overlapping Objects Recognition. *Baghdad Science Journal*, 20, 3, 893–903.

[30] Rui Zhang, Cong Xie, and Liwei Deng. 2023. A fine-grained object detection model for aerial images based on yolov5 deep neural network. *Chinese Journal of Electronics*, 32, 1, 51–63.

[31] Yongjie Zhou, Jinbo Xiong, Renwan Bi, and Youliang Tian. 2022. Secure YOLOv3-SPP; Edge-Cooperative Privacy-preserving Object Detection for Connected Autonomous Vehicles. In *2022 International Conference on Networking and Applications*. IEEE, (Dec. 2022), 82–89.

A Sub-Protocols

Algorithm 3 ConvBNSiLU, $\mathcal{F}_{ConvBNSiLU}$

Input: Parties $P_k, k \in \{0,1\}$ hold input shares $\langle x \rangle_k$, weight and bias shares $\langle W_i \rangle_k$ and $\langle b_i \rangle$ for $i \in \{0,1,2\}$
Output: P_0 and P_1 respectively hold arithmetic shares $\langle O \rangle_0$ and $\langle O \rangle_1$ of the output.

1: $P_k, k \in \{0,1\}$ compute:
$\langle t_0 \rangle_k \leftarrow \mathcal{F}_{Conv2D}(\langle x \rangle_k, \langle W_0 \rangle_k, \langle b_0 \rangle_k)$
2: $P_k, k \in \{0,1\}$ compute:
$\langle t_1 \rangle_k \leftarrow \mathcal{F}_{BatchNorm}(\langle t_0 \rangle_k, \langle W_1 \rangle_k, \langle b_1 \rangle_k)$
3: $P_k, k \in \{0,1\}$ compute: $\langle O \rangle_k \leftarrow \mathcal{F}_{Swish}(\langle t_1 \rangle_k)$

Algorithm 4 C3 Block, $\mathcal{F}_{C3}$

Input: Parties $P_k, k \in \{0,1\}$ hold input shares $\langle x \rangle_k$, weight and bias shares $\langle W_i \rangle_k$ and $\langle b_i \rangle_k$ for $i \in \{0, 1, \ldots, 2n+2\}$
Output: P_0 and P_1 respectively hold arithmetic shares $\langle O \rangle_0$ and $\langle O \rangle_1$ of the output.

1: $P_k, k \in \{0,1\}$ computes:
$\langle t_0 \rangle_k \leftarrow \mathcal{F}_{ConvBNSiLU}(\langle x \rangle_k, \langle W_0 \rangle_k, \langle b_0 \rangle_k)$ and $\langle t_1 \rangle_k \leftarrow \mathcal{F}_{ConvBNSiLU}(\langle x \rangle_k, \langle W_1 \rangle_k, \langle b_1 \rangle_k)$
2: **for** $j = 1, \ldots, n$ **do**
3: **if** Bottleneck is type 1 **then**
4: $P_k, k \in \{0,1\}$ computes:
$\langle t_0 \rangle_k \leftarrow \mathcal{F}_{Bottleneck1}(\langle t_0 \rangle_k, \langle W_{2j} \rangle_k, \langle W_{2j+1} \rangle_k, \langle b_{2j} \rangle_k, \langle b_{2j+1} \rangle_k)$
5: **else**
6: $P_k, k \in \{0,1\}$ computes:
$\langle t_0 \rangle_k \leftarrow \mathcal{F}_{Bottleneck2}(\langle t_0 \rangle_k, \langle W_{2j} \rangle_k, \langle W_{2j+1} \rangle_k, \langle b_{2j} \rangle_k, \langle b_{2j+1} \rangle_k)$
7: $P_k, k \in \{0,1\}$ computes:
$\langle t_3 \rangle_k \leftarrow \mathcal{F}_{Concat}(\langle t_0 \rangle_k, \langle t_1 \rangle_k)$
8: $P_k, k \in \{0,1\}$ computes:
$\langle O \rangle_k \leftarrow F_{ConvBNSiLU}(\langle t_3 \rangle_k, \langle W_{2n+2} \rangle_k, \langle b_{2n+2} \rangle_k)$

Algorithm 5 Bottleneck 2, $F_{Bottleneck2}$

Input: Parties $P_k, k \in \{0,1\}$ hold input shares $\langle x \rangle_k$, weight and bias shares $\langle W_i \rangle_k$ and $\langle b_i \rangle$ for $i \in \{0,1\}$
Output: P_0 and P_1 respectively hold arithmetic shares $\langle O \rangle_0$ and $\langle O \rangle_1$ of the output.

1: $P_k, k \in \{0,1\}$ computes:
$\langle t_0 \rangle_k \leftarrow \mathcal{F}_{ConvBNSiLU}(\langle x \rangle_k, \langle W_0 \rangle_k, \langle b_0 \rangle_k)$
2: $P_k, k \in \{0,1\}$ computes:
$\langle O \rangle_k \leftarrow \mathcal{F}_{ConvBNSiLU}(\langle t_0 \rangle_k, \langle W_1 \rangle_k, \langle b_1 \rangle_k)$

Algorithm 6 Bottleneck 1, $F_{Bottleneck1}$

Input: Parties $P_k, k \in \{0,1\}$ hold input shares $\langle x \rangle_k$, weight and bias shares $\langle W_i \rangle_k$ and $\langle b_i \rangle_k$ for $i \in \{0,1\}$
Output: P_0 and P_1 respectively hold arithmetic shares $\langle O \rangle_0$ and $\langle O \rangle_1$ of the output.

1: $P_k, k \in \{0,1\}$ computes:
$\langle t_0 \rangle_k \leftarrow \mathcal{F}_{ConvBNSiLU}(\langle x \rangle_k, \langle W_0 \rangle_k, \langle b_0 \rangle_k)$
2: $P_k, k \in \{0,1\}$ computes:
$\langle t_1 \rangle_k \leftarrow \mathcal{F}_{ConvBNSiLU}(\langle t_0 \rangle_k, \langle W_1 \rangle_k, \langle b_1 \rangle_k)$
3: $P_k, k \in \{0,1\}$ computes:
$\langle O \rangle_k \leftarrow \langle x \rangle_k + \langle t_1 \rangle_k$

Algorithm 7 SPPF, F_{SPPF}

Input: Parties $P_k, k \in \{0,1\}$ hold input shares $\langle x \rangle_k$, weight and bias shares $\langle W_i \rangle_k$ and $\langle b_i \rangle_k$ for $i \in \{0,1\}$
Output: P_0 and P_1 respectively hold arithmetic shares $\langle O \rangle_0$ and $\langle O \rangle_1$ of the output.

1: $P_k, k \in \{0,1\}$ computes:
$\langle t_0 \rangle_k \leftarrow \mathcal{F}_{ConvBNSiLU}(\langle x \rangle_k, \langle W_0 \rangle_k, \langle b_0 \rangle_k)$
2: $P_k, k \in \{0,1\}$ computes:
$\langle t_1 \rangle_k \leftarrow \mathcal{F}_{MaxPool2D}(\langle t_0 \rangle_k)$
3: $P_k, k \in \{0,1\}$ computes:
$\langle t_2 \rangle_k \leftarrow \mathcal{F}_{MaxPool2D}(\langle t_1 \rangle_k)$
4: $P_k, k \in \{0,1\}$ computes:
$\langle t_3 \rangle_k \leftarrow \mathcal{F}_{MaxPool2D}(\langle t_2 \rangle_k$
5: $P_k, k \in \{0,1\}$ computes:
$\langle t_4 \rangle_k \leftarrow F_{Concat}(\langle t_0 \rangle_k, \langle t_1 \rangle_k, \langle t_2 \rangle_k, \langle t_3 \rangle_k)$
6: $P_k, k \in \{0,1\}$ computes:
$\langle O \rangle_k \leftarrow F_{ConvBNSiLU}(\langle t_4 \rangle_k, \langle W_1 \rangle_k, \langle b_1 \rangle_k)$